Journal of Materials Chemistry A

Accepted Manuscript

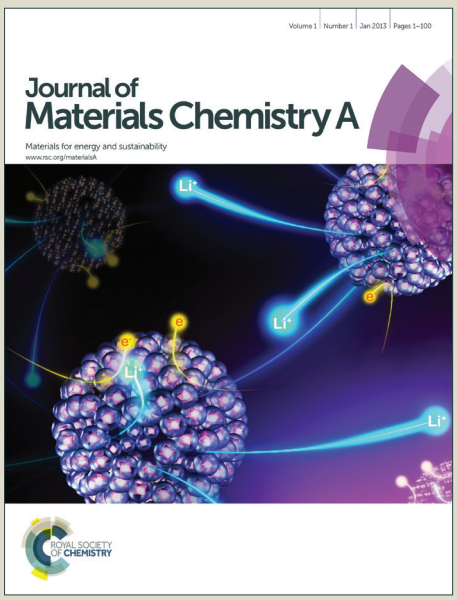

ROYAL SOCIETY OF CHEMISTRY

www.rsc.org/materialsA

Binary transition metal nitrides with enhanced activity and durability for the oxygen reduction reaction

Xinlong Tian, Junming Luo, Haoxiong Nan, Zhiyong Fu, Jianhuang Zeng, Shijun Liao*

The Key Laboratory of Fuel Cell Technology of Guangdong Province & The Key Laboratory of New Energy Technology of Guangdong Universities, School of Chemistry and Chemical Engineering, South China University of Technology, Guangzhou 510641, China

Abstract

With a novel two-step approach, we prepared a low-cost, high-performance, binary transition metal nitride (BTMN) catalyst. An ammonia (NH_3) complex of Ti and transition metal was prepared in an organic solvent by the reaction of metal ions with ammonium; the complex then was dried in a vacuum oven, followed by nitridation in a tubular furnace in NH_3 flow. The catalyst exhibited excellent activity towards the oxygen reduction reaction (ORR) in an alkaline medium and good ORR activity in an acidic medium. The effects of the doping elements (Fe, Co, and Ni), the doping concentration, and various nitriding temperatures on catalytic performance were intensively investigated. The onset potential of $Ti_{0.95}Ni_{0.5}N$ catalyst reached 0.83 V, with a limiting diffusion current density of 4 mA cm^{-2} (at a rotation speed of 1600 rpm) in 0.1 M $HClO_4$ solution, which is the highest to date among reported TiN-based electrocatalysts in an acidic medium. In 0.1 M KOH solution, the performance of this catalyst was almost comparable to that of commercial JM Pt/C; the diffusion current density reached 5.3 mA cm^{-2}, and the halfway potential was only 71 mV inferior to that of commercial JM Pt/C. Furthermore, the catalyst showed high stability and only a slight drop in its current density after durability testing. All of these findings make our BTMN catalyst attractive for PEMFCs.

Keywords: binary transition metal nitrides, titanium nitride, oxygen reduction reaction, catalyst activity, fuel cells

* Corresponding author, email: chsjliao@scut.edu.cn, fax +86 20 8711 3586

1. Introduction

Proton exchange membrane fuel cells (PEMFCs) are attractive alternatives to current energy conversion technologies owing to their high energy efficiency, high power density, relatively low operating temperature, and low emissions.[1-8] However, the commercialization of fuel cell technologies is still hampered by several challenges, including the sluggishness of the oxygen reduction reaction (ORR), electrochemical instability, and high cost, due to the use of large amounts of platinum catalyst. New electrocatalysts with high performance and durability are required, ones that can lower the over-potential and tolerate corrosive operating conditions.[8-16] In the search for alternatives to the active but expensive Pt-based ORR catalysts for PEMFCs, platinum-free catalysts have been widely explored, including metal-N [17], complexes of metal oxides and carbon materials.[9, 18-20] modified carbon nanotubes[10, 21], and doped carbonaceous materials[2, 22, 23], and promising advances have been made. Nevertheless, the current catalyst materials are still far from meeting the combined requirements of high catalytic activity, strong durability, and low cost in practical applications, especially in acidic media. New strategies to develop efficient ORR catalysts remain greatly needed.

Recently, transition metal nitrides (TMNs) have become a hot topic because they are highly electrically conductive, thermally stable, and have high melting points as well as exceptional hardness and corrosion resistance.[5, 6, 24-34] In addition, due to their desirable electrical and mechanical properties, TMNs can be used to derive advanced electrocatalysts; indeed, they have been used as supports for precious metals (like Pt and Pd) to enhance the catalysts' ORR activity and durability in comparison with commercial Pt/C catalysts.[30, 35, 36] Notably, many reports emphasize TiN nanoparticles (NPs), not only for the resulting material's excellent corrosion resistance and electrochemical stability, but also because TiN itself can act as an ORR catalyst.[6, 37, 38] The combination of TiN NPs and a carbonaceous support, such as TiN/C [5] and TiN/CNT+graphene, [38] has been reported to yield a level of ORR activity. However, little has been done to identify an optimal synthesis method and control the crystal growth of TMN NPs so as to maximize ORR

activity while maintaining electrochemical stability. What is more, numerous aspects of the ORR mechanism remain unclear. To the best of our knowledge, the synthesis of porous TiN based binary transition metal nitrides (BTMNs) nanostructures for the ORR in acidic conditions has not previously been reported.

Based on the above considerations, in this work, we synthesized BTMN NPs by combining a complexation process and a post-nitriding method, then characterized these BTMN NPs and found them to have a large surface area and fairly uniform grain size. Most importantly, our free-standing BTMN catalysts showed excellent electrochemical durability and high ORR current density, outperforming any of the single TiN-based catalysts reported to date. We also rigorously investigated the roles of composition, doping concentration, and annealing temperature and obtained some interesting results.

2. Experimental Procedures

2.1 Synthesis of BTMN catalysts

All chemicals were purchased commercially (Aladdin, China), were analytical grade or better, and were used without further purification. The BTMN NPs were prepared by a complexation approach followed by thermal treatment under ammonia (NH_3). For example, to prepare $Ti_{0.95}Ni_{0.05}N$, we first dispersed titanium tetrachloride ($TiCl_4$, 1 mL) and nickel acetate tetrahydrate ($Ni(CH_3COO)_2{\cdot}4H_2O$, 0.113 g) in 30 mL ethanol under stirring; note that we carried out this reaction under a hood because the metal precursor reacts vigorously with ethanol. After a homogeneous solution was obtained, NH_3 was introduced into it with continuous stirring for 30 min. The precipitate was then transferred to a vacuum drying oven and kept at 80°C overnight. Next, appropriate amounts of the powder precursors were placed in the tubular furnace and annealed at 700°C under an NH_3 gas flow (100 sccm min^{-1}) for 2 h using a progressive heating rate (room temperature to 680°C, 5°C min^{-1}; 680–700°C, 1°C min^{-1}), then the furnace power was turned off and the product was cooled to room temperature, still under the NH_3 gas flow. Before the product was taken out of the tubular furnace, an argon gas flow through the tube was used to expel the NH_3 gas remaining in the tube.

Finally, the product was left in the furnace for 30 min with one valve open so that the BTMN catalyst could slowly be exposed to air. Unless otherwise specified, for all the catalyst samples, the atomic ratio of the doping element to Ti was maintained at 1:19, and annealing was performed at 700°C for 2 h in an NH_3 gas flow (100 sccm min^{-1}). $Ti_{0.95}Fe_{0.05}N$ and $Ti_{0.95}Co_{0.05}N$ were prepared using the same processes as for $Ti_{0.95}Ni_{0.05}N$ but with the addition of $Fe(CH_3COO)_2$ and $Co(CH_3COO)_2{\cdot}4H_2O$ in the precursors, respectively, and TiN NPs were synthesized without the addition of any Fe, Co, or Ni precursor.

2.2 Materials characterization

X-ray diffraction (XRD) was conducted on a TD-3500 powder diffractometer (Tongda, China) operated at 30 kV and 20 mA, using Cu-Kα radiation sources and a Bragg angle ranging from 20° to 86°. Energy dispersive X-ray analysis (EDX) was performed with a field-emission scanning electron microscope (FE-SEM, Hitachi S-4800). Transmission electron microscopy (TEM) and high-resolution transmission electron microscopy (HR-TEM) images were acquired with a JEOL 2100 microscope. X-ray photoelectron spectroscopy (XPS) was performed on an Axis Ultra DLD X-ray photoelectron spectrometer employing a monochromated Al-Kα X-ray source (hv = 51486.6 eV). The Brunauer–Emmett–Teller (BET) surface area and pore distribution were measured by nitrogen adsorption–desorption on a TriStar II 3020 gas adsorption analyzer.

2.3 Electrode preparation

All electrochemical experiments were carried out on an electrochemical workstation (Ivium, Netherlands) at room temperature (25±1°C), using a three-electrode electrochemical cell with a rotating disk electrode (RDE) system (Pine Research Instrumentation, USA). The cell consisted of a glassy carbon working electrode (GCE, 5 mm inner diameter), a platinum foil counter electrode, and an Ag/AgCl (saturated 3M NaCl) reference electrode. All potentials in this work are quoted with respect to the reversible hydrogen electrode (RHE). The catalyst electrode was prepared as follows: first, a catalyst ink was prepared

by ultrasonicating a mixture of 5.0 mg BTMN catalyst without adding any conductive carbon materials, and 1 mL Nafion (0.25 wt%) ethanol solution for 30 min. Subsequently, 20 μL catalyst ink was pipetted onto the GCE surface. Finally, the GCE was dried under an infrared lamp for 5 min. The loading for every BTMN catalyst was calculated to be 0.5 mg cm^{-2}, while the Pt loading for the JM Pt/C catalyst (3.3 nm, 20 wt% Pt supported on Vulcan XC-72R carbon) was 25 μg cm^{-2}.

Cyclic voltammetry (CV) characterization of the catalysts in the absence of oxygen was typically carried out in a potential range from 0.1 to 1.3 V at a scan rate of 50 mV s^{-1} in N_2-saturated 0.1 M $HClO_4$ solution. The ORR polarization curves were recorded in O_2-saturated 0.1 M $HClO_4$ electrolyte at a rotation rate of 1600 rpm and a scan rate of 10 mV s^{-1}. An accelerated durability test (ADT) was performed on the catalysts in O_2-saturated 0.1 M $HClO_4$ and 0.1 M KOH by chronoamperometric method for 30, 000 s at 0.7 V at room temperature.

3. Results and discussion

Fig. 1 compares the XRD patterns of several samples as prepared from various precursors. The diffraction peaks of the synthesized TiN NPs, centered at 36.7°, 42.6°, 61.8°, 74.1°, and 77.9°, correspond to the face centered cubic (fcc) structure of TiN (JCPDS No. 38-1420). [26] After the nitridation process, only the fcc TiN phase could be observed for all of the BTMNs, and the locations of the diffraction peaks were almost identical to those of TiN NPs, except for a slight shift toward a higher 2θ angle. This phenomenon indicates a partial substitution of Ti atoms with the doping atoms, which possess a smaller atomic radius. Furthermore, no signals corresponding to a single metallic phase or to the oxide or nitride phases of the doping elements were detected, suggesting that the BTMNs were formed as a highly pure, single-phase solid solution. Using the Scherrer equation, we estimated the average particle sizes of the TMNs to be 9.8, 10.8, 9.7, and 9.2 nm for TiN, $Ti_{0.95}Fe_{0.05}N$, $Ti_{0.95}Co_{0.05}N$, and $Ti_{0.95}Ni_{0.05}N$, respectively. The EDX profiles of all of the BTMN samples are shown in Table 1, and every sample was recorded for three different areas. The

average atomic ratio for all of the BTMNs was consistent with the atomic ratio of 19:1 used in the precursors, implying that the composition of these BTMNs can be adjusted in a facile manner by tuning the ratio of the doping precursor and $TiCl_4$ in the synthesis process.

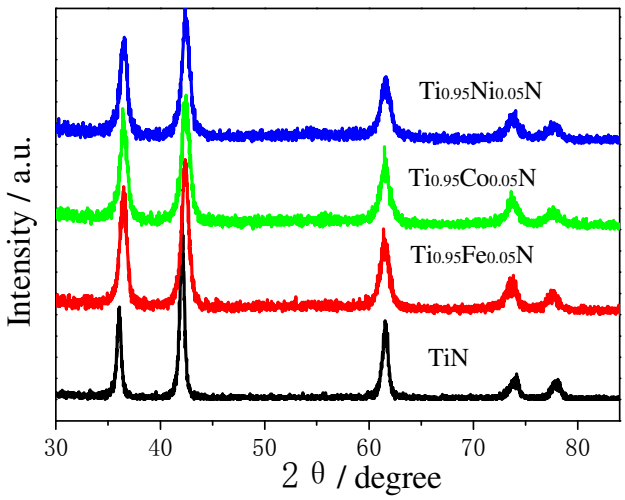

Fig. 1. XRD patterns of as-prepared TiN, $Ti_{0.95}Fe_{0.05}N$, $Ti_{0.95}Co_{0.05}N$, and $Ti_{0.95}Ni_{0.05}N$ NPs.

Table 1. EDX profile and grain size of $Ti_{0.95}Fe_{0.05}N$, $Ti_{0.95}Co_{0.05}N$, and $Ti_{0.95}Ni_{0.05}N$.

Sample	Ti at%	Doped metal at%	Grain size (nm)
$Ti_{0.95}Fe_{0.05}N$	47.5	2.54	10.8
$Ti_{0.95}Co_{0.05}N$	47.4	2.67	9.7
$Ti_{0.95}Ni_{0.05}N$	46.9	2.50	9.2

TEM images of the synthesized TiN and BTMNs are exhibited in Fig. 2. Aggregates of uniform TMN NPs with spherical shapes were observed, and the structure and morphology of the TMN NPs were slightly affected by the doping of various transition metals. The detailed structural features of all samples were characterized by HR-TEM, as shown in the insets in Fig. 2(a–d). The clear fringes revealed the single-crystal nature of the crystals, and the lattice spacing of ca. 0.251 nm corresponded well to a growth direction along the (111) plane of fcc TiN.[26] The HR-TEM findings were consistent with the XRD results, which suggested that all the TMNs were formed as single-phase solid solutions.

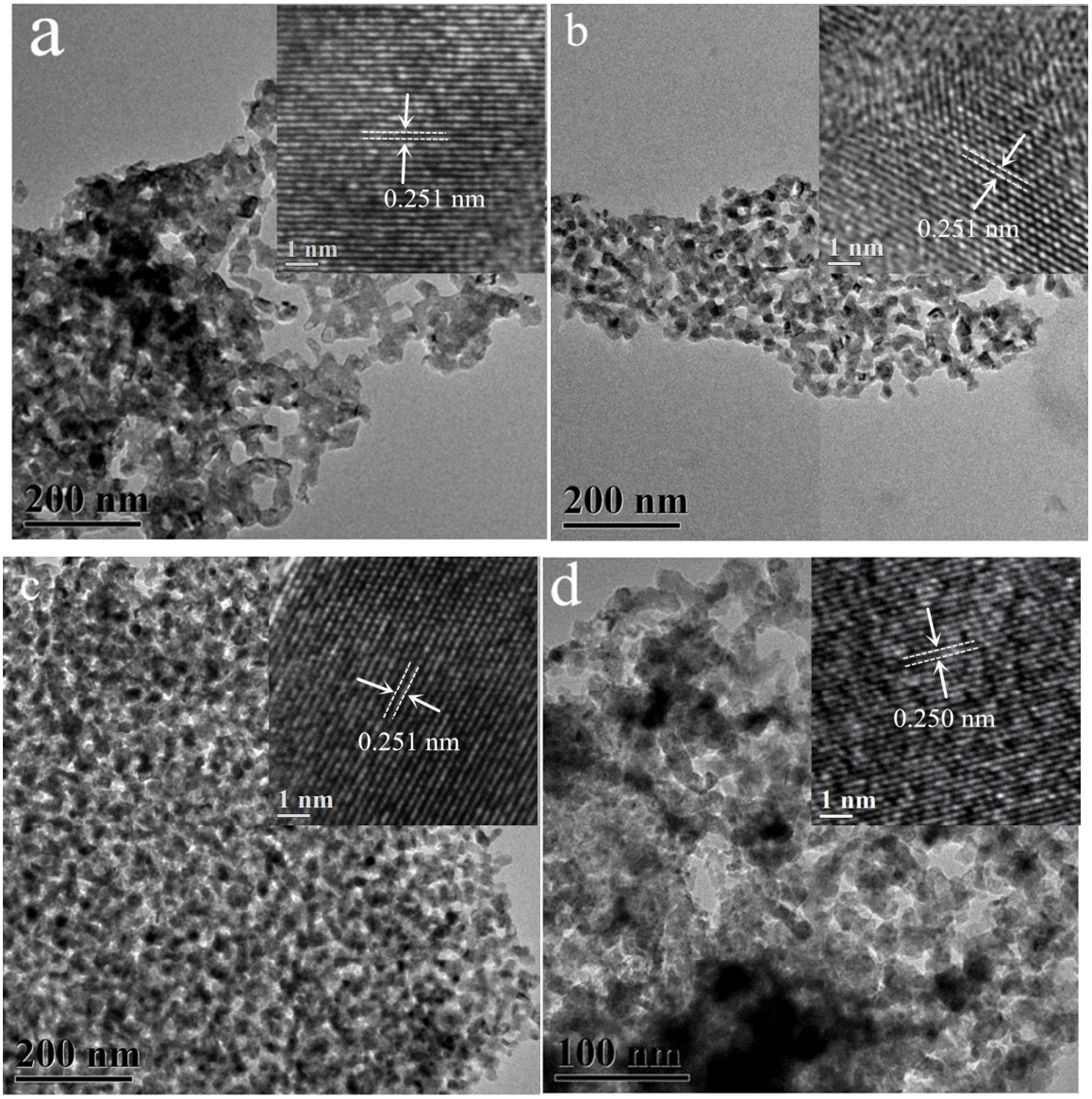

Fig. 2. TEM images of (a) TiN, (b)$Ti_{0.95}Fe_{0.05}N$, (c)$Ti_{0.95}Co_{0.05}N$, and (d)$Ti_{0.95}Ni_{0.05}N$. The inset in each is the corresponding HR-TEM image.

To further study the doping effects of various transition metals, we measured the nitrogen adsorption–desorption isotherms and calculated the corresponding Barrett–Joyner–Halenda (BJH) pore size distributions of the TMNs, as shown in Fig. 3. Fig. 3a shows that doping with the various metals had a significant effect on the surface area. The BTMN catalyst doped with Ni exhibited the highest surface area (286 $m^2 g^{-1}$), compared with 143, 119 and 189 $m^2 g^{-1}$ for TiN, $Ti_{0.95}Fe_{0.05}N$ and $Ti_{0.95}Co_{0.05}N$, respectively,

due to it having smaller NPs than the other BTMNs. Although all of the BTMNs exhibited a similar structure and morphology (Fig. 2), they had obviously different pore volumes (Fig. 3b), suggesting that the various doping agents had strong effects on the catalysts' microstructures.

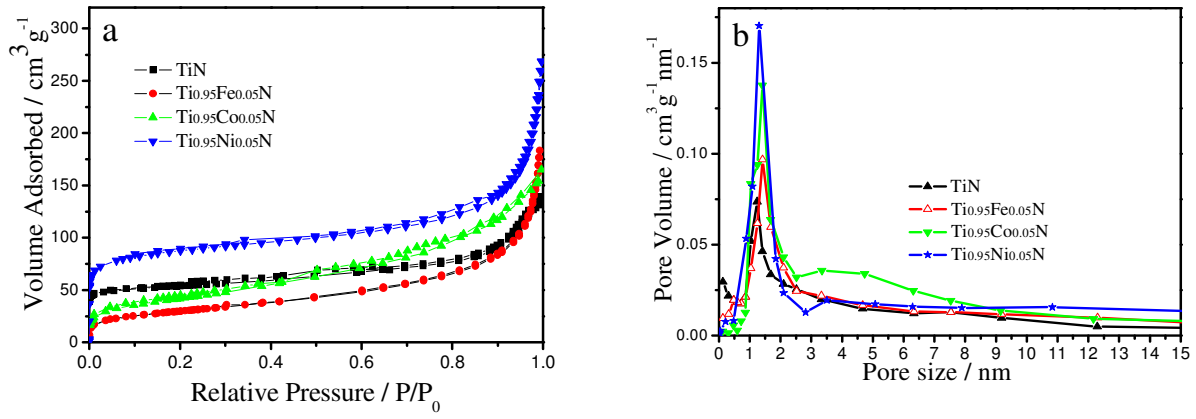

Fig. 3. (a) N_2 adsorption–desorption isotherms; (b) Barrett–Joyner–Halenda adsorption pore size distributions of TiN, $Ti_{0.95}Fe_{0.05}N$, $Ti_{0.95}Co_{0.05}N$, and $Ti_{0.95}Ni_{0.05}N$.

The electrochemical stability of the TiN and BTMNs was investigated using CV. We tested the samples over a potential range of 0.1–1.3 V at a scan rate of 50 mV s^{-1} in a 0.1 M $HClO_4$ solution for 20 scans at room temperature, as shown in Fig. 4. No special redox currents were observed in their CV traces, demonstrating that all of the TMN catalysts exhibited high electrochemical stability.

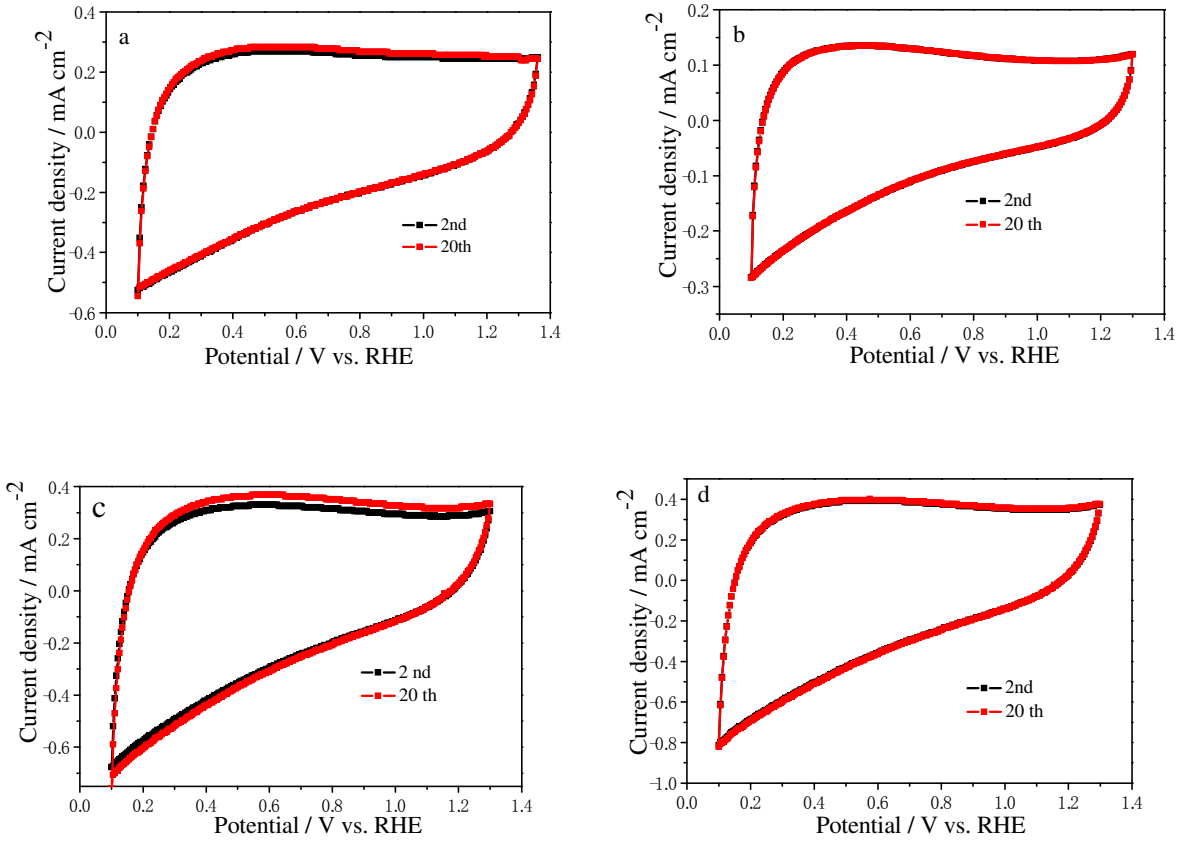

Fig. 4. CVs of (a) TiN, (b) $Ti_{0.95}Fe_{0.05}N$, (c) $Ti_{0.95}Co_{0.05}N$, and (d) $Ti_{0.95}Ni_{0.05}N$ catalysts in N_2-saturated 0.1 M $HClO_4$ solution at a scan rate of 50 mV s^{-1}

Fig. 5a shows the activity of the catalysts toward the ORR in O_2-saturated 0.1 M $HClO_4$. The activity of TiN was so poor that the current density reached only 0.13 mA cm^{-2} at 0.7 V. However, when another transition metal was introduced, the activity dramatically improved, suggesting that the BTMN catalysts were much more active than the TiN towards the ORR. As shown in Fig. 5 a and b, the ORR onset potential and activity for the BTMNs followed the order Ni > Co > Fe > TiN in both acidic and alkaline media. For $Ti_{0.95}Ni_{0.5}N$, the onset potential was up to 0.85 V and the current density reached 2.63 mA cm^{-2} (0.7 V vs. RHE) in acidic conditions. It should be noted that the onset potential and half-wave potential of $Ti_{0.95}Ni_{0.5}N$ were 0.12 and 0.17 V lower than those of commercial JM Pt/C catalyst. Nonetheless, the performance of our catalyst was still excellent, because it surpassed all other reported TiN-based electrocatalysts [5, 37, 38], and it is

very difficult to obtain a desirable result using a Pt-free catalyst in an acidic medium.[39, 40] It is interesting that the order of the ORR activity for the BTMNs was exactly consistent with their surface area order, suggesting that the essential activity of these BTMNs catalysts may have a common cause—namely, that the number of active sites increases with decreasing particle size. Notably, although the surface area of TiN was larger than that of $Ti_{0.95}Fe_{0.05}N$, the former's ORR activity was far inferior, further confirming that the BTMN catalysts were more active towards the ORR than the single TiN NPs. Additionally, if we normalized the current density (0.7 V) to the BET surface area, we found that the $Ti_{0.95}Ni_{0.05}N$ still exhibited the highest specific surface area activity toward the ORR and TiN the lowest (Fig. S1, ESI), revealing that the highest performance of $Ti_{0.95}Ni_{0.05}N$ may be caused not only by its high surface area, but also its high intrinsic activity. Furhermore, we also evaluated the catalysts with graphite electrode instead of platinum wire as counter electrode in order to exclude the possible Pt dissolution, and no obvious variation of the results can be observed between the two type of counter electrodes (Fig. S2, ESI).

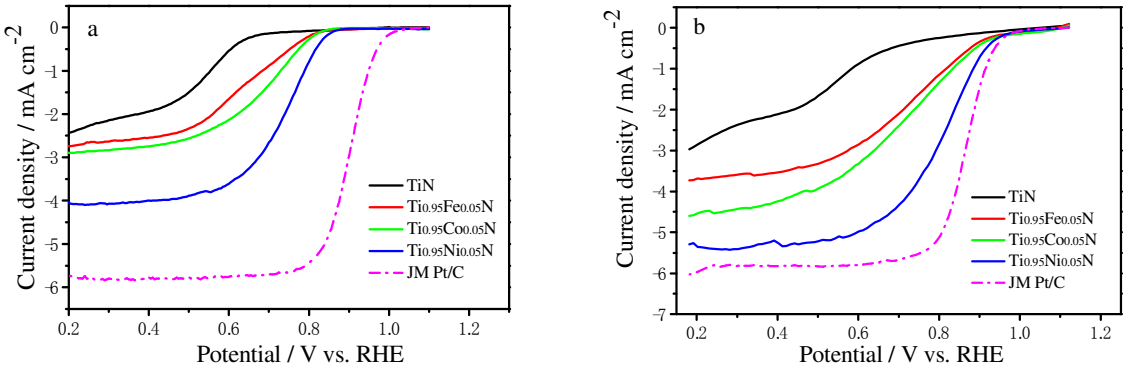

Fig. 5 Linear sweep voltammetry curves of TiN, $Ti_{0.95}Fe_{0.05}N$, $Ti_{0.95}Co_{0.05}N$, and $Ti_{0.95}Ni_{0.05}N$ in (a) O_2-saturated 0.1 M $HClO_4$ and (b) 0.1 M KOH.

The electron transfer number, n, of each of the BTMN catalysts was derived from the slopes of the Koutecky–Levich plots at various potentials, as shown in Fig. 6 a and b. For TiN catalyst, the value of n is 2.0, 2.0, 2.1, 2.2, 2.4 with the potential of 0.62, 0.58, 0.54, 0.50 and 0.47 V, respectively, indicating that the

catalysis process predominantly followed the two-electron transfer pathway. However, for $Ti_{0.95}Ni_{0.05}N$, at low overpotential (0.74 V), n≈3.4 was calculated, indicating both two- and four-electron reductions taking place. When the potential was polarized in the more negative direction, n increased to approach 3.9 at 0.55 V (Fig. 6b), suggesting nearly four-electron reduction of O_2 in this potential region on the $Ti_{0.95}Ni_{0.05}N$ catalyst. For $Ti_{0.95}Fe_{0.05}N$ and $Ti_{0.95}Co_{0.05}N$ catalysts, the values of n were shown in Fig. S3 with various potential, and the values indicated the coexistence of two- and four-electron reductions pathway. Thus, the BTMN catalysts exhibit higher ORR performance and limiting diffusion current density than that of TiN only.

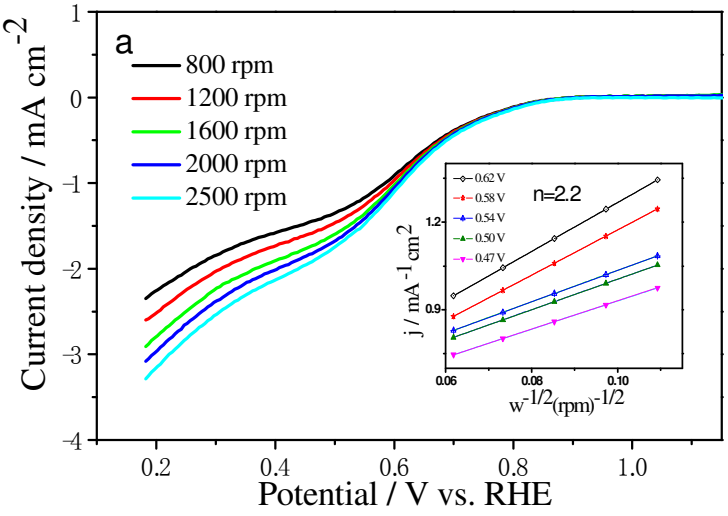

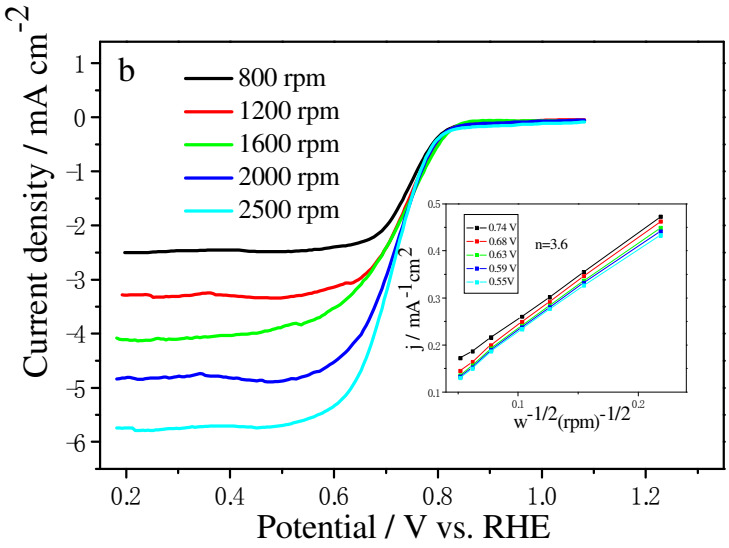

Fig. 6. (a) ORR polarization plots of (a) TiN and (b) $Ti_{0.95}Ni_{0.05}N$ in O_2-saturated 0.1 M $HClO_4$ electrolytes at different rotation rates, and (insert) the Koutecky–Levich plots.

To understand if the superior ORR catalytic activity of $Ti_{0.95}Ni_{0.05}N$ is a result of the different electronic properties due to Ni doping, XPS spectra of the BTMN were collected and shown in Fig. 7. Fig. 7(a–c) shows the XPS spectra of Fe 2p, Co 2p, and Ni 2p for $Ti_{0.95}Fe_{0.05}N$, $Ti_{0.95}Co_{0.05}N$, and $Ti_{0.95}Ni_{0.05}N$, respectively. For the Fe-doped catalyst, the XPS spectrum revealed the coexistence of Fe(II) and Fe(III), which may correspond to Fe-N bonding in the $Ti_{0.95}Fe_{0.05}N$ structure [3, 41]. In the spectrum of the Co-doped catalyst, the peaks at 780.3 (795.3) and 784.7 (797.6) eV correspond to Co and Co-N[42], respectively. The Ni $2p_{3/2}$ and Ni $2p_{1/2}$ electron spectra show primary signals at 855.6 and 873.4 eV, plus satellites at 860.9 and 879.5 eV, respectively. The binding energies and separation of the 2p doublet may correspond to NiO[43], and they suggest that the surface Ni of $Ti_{0.95}Ni_{0.05}N$ is predominantly found as Ni^{2+}. In principle, the general agreement concerning the direction of charge transfer in nitrides is from metal to N atoms[44], this is further supported by our results, which show that the spectra of Ti 2p in all the catalysts was shifted to higher binding energies with respect to pure Ti metal (Ti 2p, 456 eV), as presented in Fig. 7 d. As we know, charge transfer from Ti to N atoms will lead to an increase in the Ti d-band vacancy.[44] Interestingly, there was a

clear negative shift of Ti 2p for all the BTMNs compared with the TiN, yet without the N 1s spectra almost unchanged (Fig. S4a, ESI). An apparent negative shift of ca. 0.27, 0.39 and 0.48 eV in the binding energy of Ti $2p_{3/2}$ of $Ti_{0.95}Fe_{0.05}N$, $Ti_{0.95}Co_{0.05}N$, and $Ti_{0.95}Ni_{0.05}N$, respectively, relative to that of the TiN catalyst were observed (Fig. S4b, ESI), indicating that the Ti atoms of the BTMNs received electrons donated from the doped transition metal and the electrons number increased with increasing electro-negativity of the doping metals (Ni >Co >Fe). This electron compensation directly reflects a decrease in the d-band vacancy of Ti atoms, leading to an increase in the extent of Ti d-band occupation near the Fermi level. It is reasonable to propose that the increase in the d-band occupation of the BTMN catalysts conferred an enhanced ability to donate d electrons to the adsorbed oxygen, and thus the ORR performance was improved; certainly the BTMNs exhibited better performance toward the ORR than TiN.

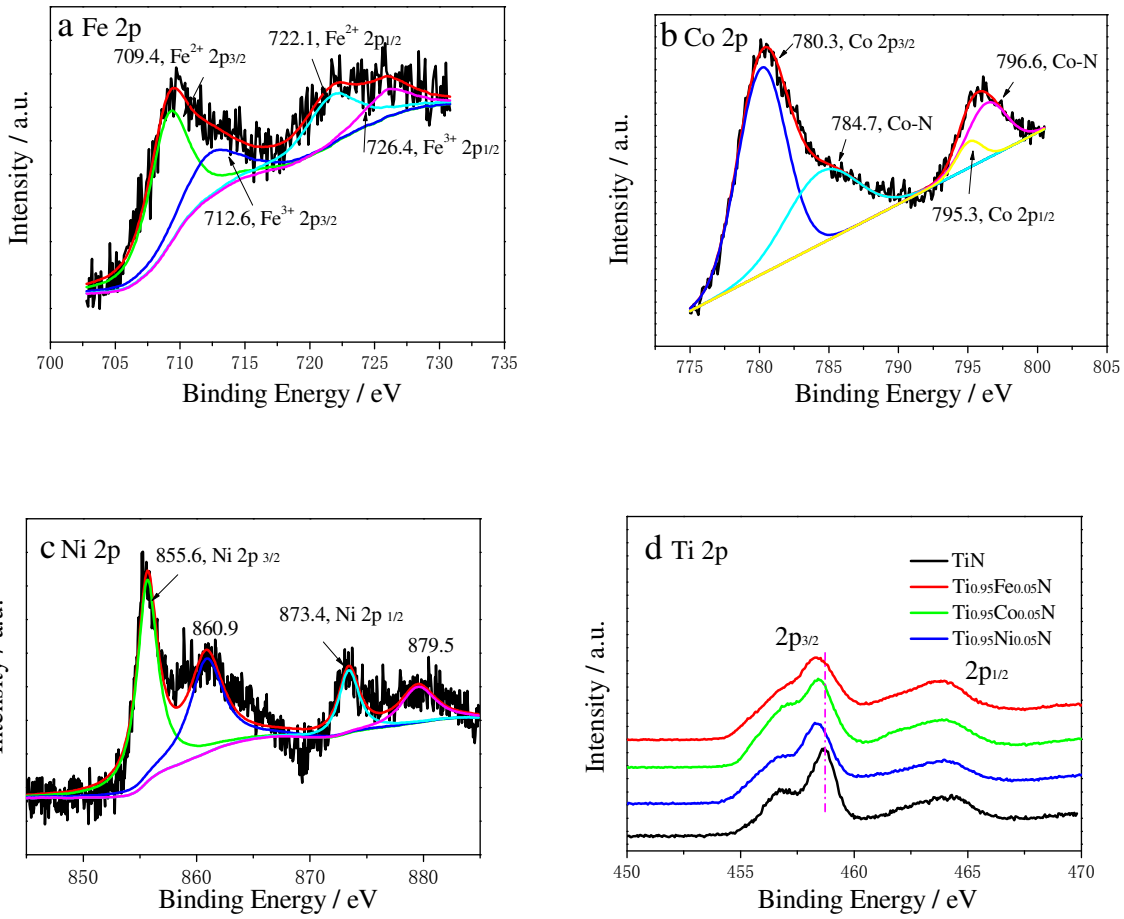

Fig. 7. High-resolution XPS spectra of (a) Fe 2p for $Ti_{0.95}Fe_{0.05}N$, (b) Co 2p for $Ti_{0.95}Co_{0.05}N$, (c) Ni 2p for $Ti_{0.95}Ni_{0.05}N$, and (d) Ti 2p for TiN, $Ti_{0.95}Fe_{0.05}N$, $Ti_{0.95}Co_{0.05}N$, and $Ti_{0.95}Ni_{0.05}N$, respectively.

On the other hand, there is an alternative but complementary explanation for the observed activity enhancement in BTMNs compared with TiN. A previous study noted the phenomenon of a "volcano plot," in which the M-O bond strength exhibits an ascending branch followed by a descending branch [45]. Titanium binds O atoms strongly, whereas nickel binds them weakly; the order of strength is Ti > Fe > Co > Ni. We suggest that doping with Fe, Co, or Ni might modify the strength between the Ti and O atoms, especially in the case of Ni doping, leading to a relatively moderate Ti–O binding strength, which would definitely aid in the removal of oxygenated intermediates from the surface of $Ti_{0.95}Ni_{0.05}N$, and in turn strengthening the ORR activity. It should be noted that this proposed mechanism of enhanced activity must be considered preliminary, as a comprehensive study of the activity mechanism is needed. Although it is beyond the scope of the present work, additional insights into the physicochemical origins of the enhanced ORR performance of BTMNs can be obtained by techniques such as X-ray absorption near-edge spectroscopy (XANES), which can likely supply more detailed information regarding surface structure and elemental chemical states. We intend to conduct these characterization experiments in the near future.

Fig. 8a shows the effects of annealing temperature on the performance of $Ti_{0.95}Ni_{0.05}N$. The optimal temperature appeared to be 700°C. Below that, the final product was a mixture of anatase TiO_2 and TiNiN (Fig. 8b), indicating that the precursors could not be completely converted to TiNiN. However, going above that annealing temperature caused degradation of the porous structures, as is evident in the BET measurements (Fig. 8c) and TEM image (Fig. S5, ESI). Therefore, temperatures above 700°C yielded lower ORR activity.

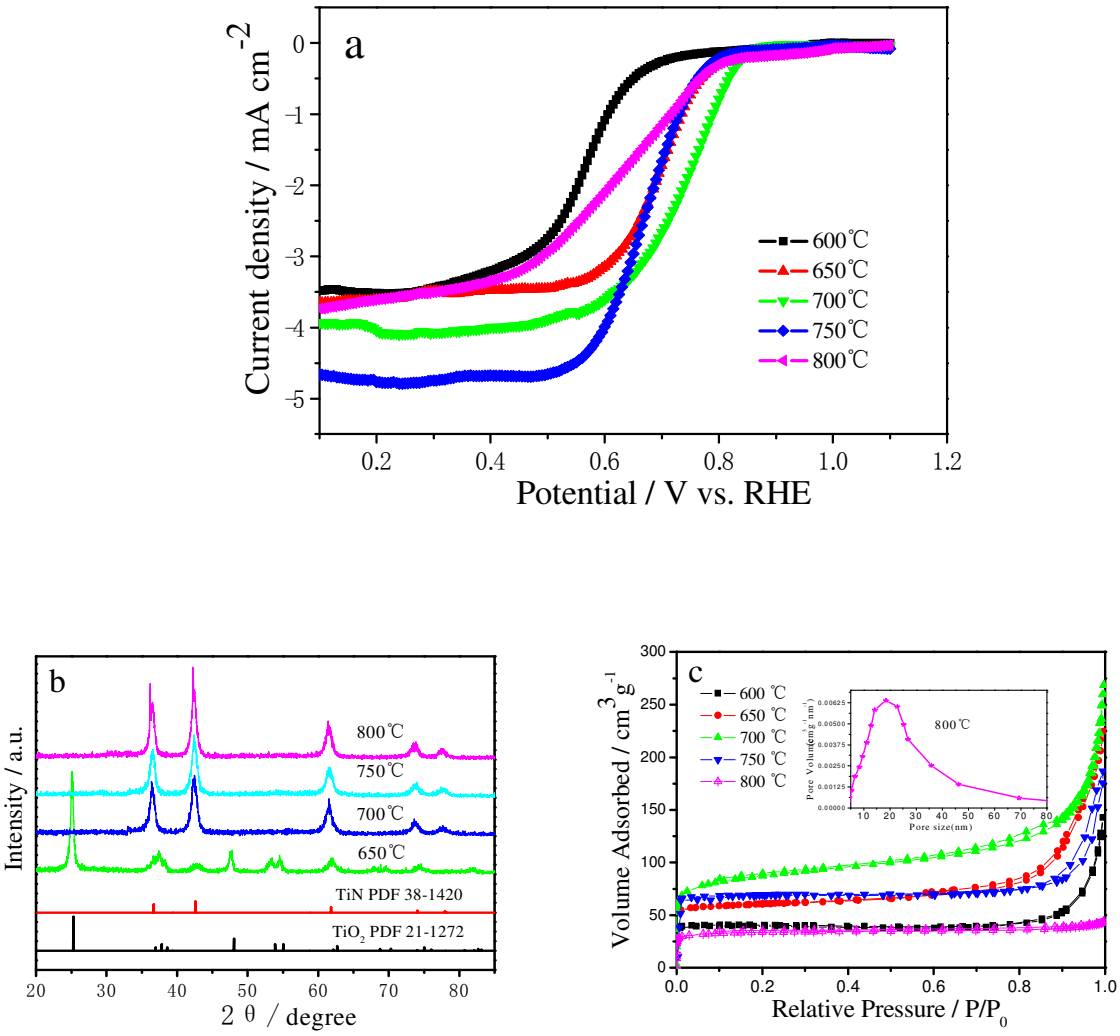

Fig. 8. (a) Linear sweep voltammetry curves of $Ti_{0.95}Ni_{0.05}N$ in O_2-saturated 0.1 M $HClO_4$, (b) XRD patterns of $Ti_{0.95}Ni_{0.05}N$, (c) N_2 adsorption–desorption isotherms of $Ti_{0.95}Ni_{0.05}N$ for various annealing temperatures.

The effects of various doping concentrations on the ORR activity of $Ti_{0.95}Ni_{0.05}N$ are presented in Fig. 9a. When nickel was introduced, the activity dramatically improved. When the doping concentration was lower than 5%, the greater the nickel addition, the higher the activity. As discussed earlier, we suppose that the lower d-band occupation near the Fermi level of Ti atoms can be compensated by nickel doping, and then $Ti_{0.95}Ni_{0.05}N$ surface has an enhanced ability to donate d electrons to adsorbed O_2 molecules, resulting

in better ORR activity, and this ability can be strengthened by increasing the amount of nickel doping. However, phase separation between TiN/$Ti_{0.95}Ni_{0.05}N$ and NiN was observable when the doping concentration was increased to 7% (Fig. 9b). The mixture became electrochemically unstable (Fig. 9c), leading to lower ORR activity.

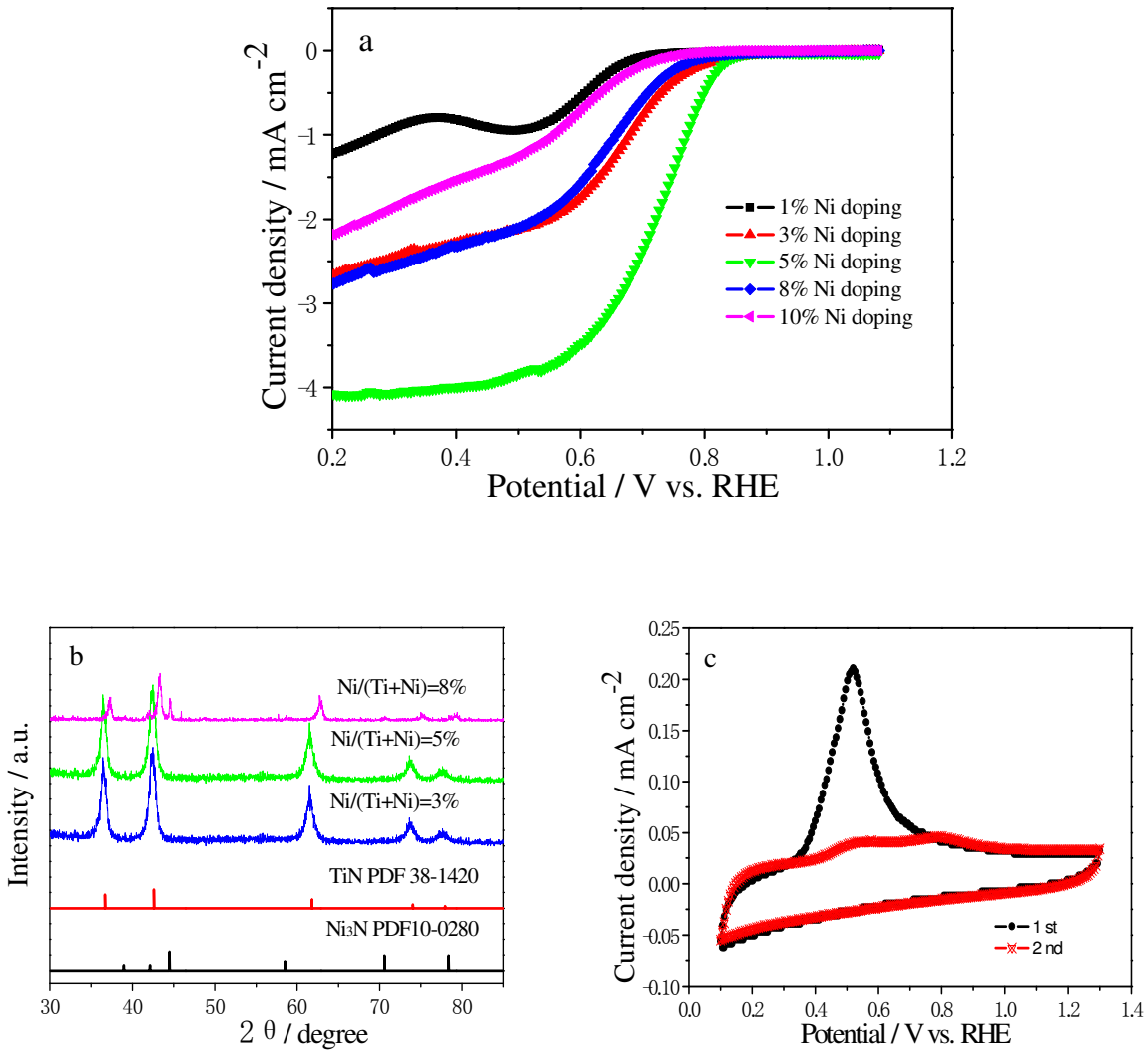

Fig. 9. (a) Linear sweep voltammetry curves of $Ti_{0.95}Ni_{0.05}N$ in O_2-saturated 0.1 M $HClO_4$, (b) XRD patterns of $Ti_{0.95}Ni_{0.05}N$, and (c) CVs of $Ti_{0.95}Ni_{0.05}N$ with various doping concentrations.

An efficient ORR catalyst is needed for both PEMFCs and direct methanol fuel cells (DMFCs). For application in DMFCs, the catalyst should satisfy tolerance to methanol that crossed from the anode side

through the membrane. As shown in Fig. S6, after the addition of 5.0 ml mixed solutions (0.1 M KOH + 3 M methanol) into the electrolyte (ca. 50 ml), the ORR current density for the $Ti_{0.95}Ni_{0.05}N$ catalyst exhibits no variation in its traces. On the contrary, the ORR current density for the Pt/C catalyst suffers a drastic decrease, demonstrating that $Ti_{0.95}Ni_{0.05}N$ catalyst has excellent methanol tolerance.

Electrocatalyst durability remains one of the most important issues to be resolved before fuel cells can become commercially available. Fig. 10a shows the results of our chronoamperometric durability test for the ORR in O_2-saturated 0.1 M $HClO_4$ and KOH solution, respectively, conducted for 30,000 s at 0.7 V. We observed only 13.5% loss in current density and a negative shift of 15 mV in half-wave potential compared with the initial sample, demonstrating the excellent electrochemical durability of $Ti_{0.95}Ni_{0.05}N$ catalyst in acidic conditions. Furthermore, the catalyst exhibits superb stability in 0.1 M KOH solution, and almost no activity variation was observed after the durability test (Fig. 10b).

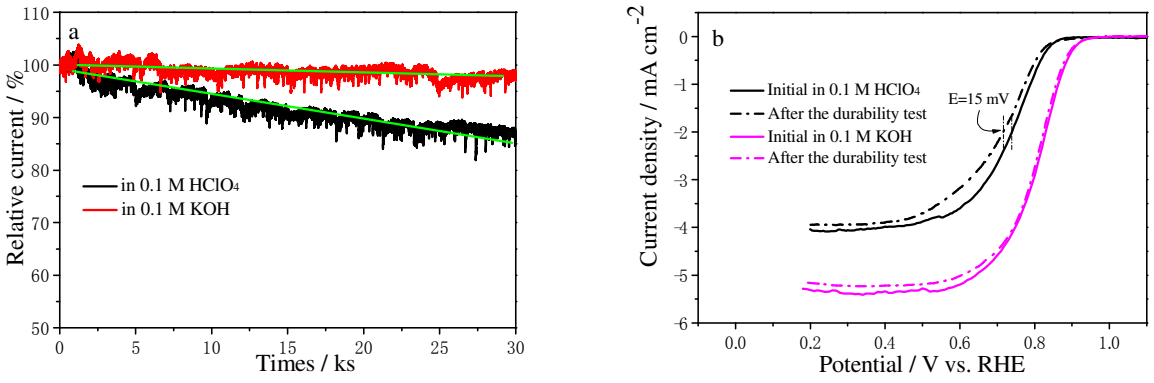

Fig. 9. (a) Chronoamperometric response for the ORR at $Ti_{0.95}Ni_{0.05}N$ electrodes: durability evaluation of $Ti_{0.95}Ni_{0.05}N$ for 30,000 s at 0.7 V and a rotation rate of 900 rpm, in O_2-saturated 0.1 M $HClO_4$ and 0.1 M KOH, (b) Polarization curves of $Ti_{0.95}Ni_{0.05}N$ before (solid curves) and after (dashed curves) the durability test.

Moreover, to gain the understanding of the durability of $Ti_{0.95}Ni_{0.05}N$ catalyst, the catalyst were collected after the durability test by sonicating the GCE in ethanol, and their structures were observed by

TEM. As shown in Fig. S7, no significant morphological change was observed after the durability test, and the nanostructures were excellently retained. The EDX profiles of $Ti_{0.95}Ni_{0.05}N$ catalyst before and after the durability test were represented in Fig. S8a and b, respectively. The atomic percentage of Ni was only decreased by approximately 5% throughout the continuous cycling, which indicates the Ni leaching was prevented by this doping method. Furthermore, the increase of O atoms was observed when compared with the initial sample, which may be due to the existence of TiO_2 species on the surface of the catalyst, and the XRD data presented in Fig. S9 shows evidence of only fcc TiN phase after the stability test, confirming that the amount of TiO_2 is trace or the surface layer is very thin. We suspect that the TiO_2-existed surface (perhaps with some contribution from TiON) is responsible for the stability and the ORR catalytic activity degradation of $Ti_{0.95}Ni_{0.05}N$ catalyst over extended test times, since TiO_2 is stable but inactive.

4. Conclusions

In summary, we have developed a robust, free-standing BTMN catalyst that demonstrates high activity and durability for the ORR under acidic conditions, and which is projected to be less expensive than commercial Pt/C catalyst and easier to synthesize. The experimental data indicated that the doping may have had (i) a "compensation effect" that enhanced the ability of Ti atoms to donate d electrons to adsorbed oxygen molecules, and (ii) a "modification effect" that tuned the Ti-O strength to a moderate degree, both of which contributed to the improved activity of the BTMN catalysts. Most importantly, $Ti_{0.95}Ni_{0.05}N$ exhibited much better ORR activity than any other previously reported TiN-based catalyst. The synthesis of inexpensive BTMNs introduces the possibility of designing a novel catalyst system for a wide range of applications in energy conversion processes.

Electronic Supplementary Information (ESI) Available

The high-resolution N 1s spectra, and the enlarged Ti $2p_{3/2}$ part of TiN, $Ti_{0.95}Fe_{0.05}N$, $Ti_{0.95}Co_{0.05}N$,

and $Ti_{0.95}Ni_{0.05}N$, TEM image of and enlarged TEM image of $Ti_{0.95}Ni_{0.05}N$ annealed at 800°C, Chronoamperometric response for the ORR of $Ti_{0.95}Ni_{0.05}N$ and Pt/C electrodes with the addition of methanol to the electrolyte after about 230 s at 0.7 V, TEM and enlarged TEM images of $Ti_{0.95}Ni_{0.05}N$ after the durability test, the EDX profiles of $Ti_{0.95}Ni_{0.05}N$ catalyst before and after the durability test, and XRD pattern of $Ti_{0.95}Ni_{0.05}N$ after the durability test.

Acknowledgements

This work was supported by the National Science Foundation of China (NSFC Project Nos. 21076089, 21276098, 11132004, and U1301245), the Guangdong Natural Science Foundation (Project No. S2012020011061), the Doctoral Fund of the Ministry of Education of China (20110172110012), and the Doctoral Fund of the Department of Education of Guangdong.

References

1. R. Zheng, Z. Mo, S. Liao, H. Song, Z. Fu and P. Huang, *Carbon*, 2014, **69**, 132-141.
2. H. Peng, Z. Mo, S. Liao, H. Liang, L. Yang, F. Luo, H. Song, Y. Zhong and B. Zhang, *Scientific reports*, 2013, **3**.
3. H. Peng, S. Hou, D. Dang, B. Zhang, F. Liu, R. Zheng, F. Luo, H. Song, P. Huang and S. Liao, *Applied Catalysis B: Environmental*, 2014, **158-159**, 60-69.
4. Y. Liu and W. E. Mustain, *Journal of the American Chemical Society*, 2013, **135**, 530-533.
5. J. Chen, K. Takanabe, R. Ohnishi, D. Lu, S. Okada, H. Hatasawa, H. Morioka, M. Antonietti, J. Kubota and K. Domen, *Chemical communications*, 2010, **46**, 7492-7494.
6. B. Avasarala, T. Murray, W. Li and P. Haldar, *Journal of Materials Chemistry*, 2009, **19**, 1803.
7. B. Y. Xia, B. Wang, H. B. Wu, Z. Liu, X. Wang and X. W. Lou, *Journal of Materials Chemistry*, 2012, **22**, 16499.

8. B. Y. Xia, N. Wan Theng, H. B. Wu, X. Wang and X. W. Lou, *Angewandte Chemie-International Edition*, 2012, **51**, 7213-7216.

9. Y. Liang, H. Wang, P. Diao, W. Chang, G. Hong, Y. Li, M. Gong, L. Xie, J. Zhou, J. Wang, T. Z. Regier, F. Wei and H. Dai, *Journal of the American Chemical Society*, 2012, **134**, 15849-15857.

10. Y. Li, W. Zhou, H. Wang, L. Xie, Y. Liang, F. Wei, J. C. Idrobo, S. J. Pennycook and H. Dai, *Nature nanotechnology*, 2012, **7**, 394-400.

11. C. You, S. Liao, H. Li, S. Hou, H. Peng, X. Zeng, F. Liu, R. Zheng, Z. Fu and Y. Li, *Carbon*, 2014, **69**, 294-301.

12. K. A. Kuttiyiel, K. Sasaki, Y. Choi, D. Su, P. Liu and R. R. Adzic, *Nano Lett*, 2012, **12**, 6266-6271.

13. H. Liu, C. Koenigsmann, R. R. Adzic and S. S. Wong, *Acs Catalysis*, 2014, **4**, 2544-2555.

14. Y. Li, Y. Li, E. Zhu, T. McLouth, C. Y. Chiu, X. Huang and Y. Huang, *Journal of the American Chemical Society*, 2012, **134**, 12326-12329.

15. K. Huang, K. Sasaki, R. R. Adzic and Y. Xing, *Journal of Materials Chemistry*, 2012, **22**, 16824.

16. B. Lim, M. Jiang, P. H. Camargo, E. C. Cho, J. Tao, X. Lu, Y. Zhu and Y. Xia, *Science*, 2009, **324**, 1302-1305.

17. H. Yin, C. Zhang, F. Liu and Y. Hou, *Advanced Functional Materials*, 2014, **24**, 2930-2937.

18. J. Xu, P. Gao and T. S. Zhao, *Energy & Environmental Science*, 2012, **5**, 5333.

19. M. Wang, J. Huang, M. Wang, D. Zhang, W. Zhang, W. Li and J. Chen, *Electrochemistry Communications*, 2013, **34**, 299-303.

20. Y. Liang, Y. Li, H. Wang, J. Zhou, J. Wang, T. Regier and H. Dai, *Nature materials*, 2011, **10**, 780-786.

21. D. Deng, L. Yu, X. Chen, G. Wang, L. Jin, X. Pan, J. Deng, G. Sun and X. Bao, *Angewandte Chemie*, 2013, **52**, 371-375.

22. Z. Mo, R. Zheng, H. Peng, H. Liang and S. Liao, *Journal of Power Sources*, 2014, **245**, 801-807.

23. L. Zhang and Z. Xia, *The Journal of Physical Chemistry C*, 2011, **115**, 11170-11176.

24. G. R. Li, F. Wang, Q. W. Jiang, X. P. Gao and P. W. Shen, *Angewandte Chemie*, 2010, **49**, 3653-3656.

25. L. Jiang and L. Gao, *Journal of Materials Chemistry*, 2005, **15**, 260.

26. Y. Dong, Y. Wu, M. Liu and J. Li, *ChemSusChem*, 2013, **6**, 2016-2021.

27. B. Avasarala and P. Haldar, *International Journal of Hydrogen Energy*, 2011, **36**, 3965-3974.

28. B. Avasarala and P. Haldar, *Energy*, 2013, **57**, 545-553.

29. M. Yang, R. Guarecuco and F. J. DiSalvo, *Chemistry of Materials*, 2013, **25**, 1783-1787.

30. M. Yang, Z. Cui and F. J. DiSalvo, *Physical Chemistry Chemical Physics*, 2013, **15**, 1088-1092.

31. M. M. O. Thotiyl, T. R. Kumar and S. Sampath, *Journal of Physical Chemistry C*, 2010, **114**, 17934-17941.

32. M. M. Ottakam Thotiyl, T. Ravikumar and S. Sampath, *Journal of Materials Chemistry*, 2010, **20**, 10643.

33. M. M. O. Thotiyl and S. Sampath, *Electrochimica Acta*, 2011, **56**, 3549-3554.

34. A. Seifitokaldani, O. Savadogo and M. Perrier, *Electrochimica Acta*, 2014, **141**, 25-32.

35. B. Avasarala and P. Haldar, *Electrochimica Acta*, 2010, **55**, 9024-9034.

36. R. Kumar, S. Pasupathi, B. G. Pollet and K. Scott, *Electrochimica Acta*, 2013, **109**, 365-369.

37. R. Ohnishi, K. Takanabe, M. Katayama, J. Kubota and K. Domen, *The Journal of Physical Chemistry C*, 2013, **117**, 496-502.

38. D. H. Youn, G. Bae, S. Han, J. Y. Kim, J.-W. Jang, H. Park, S. H. Choi and J. S. Lee, *Journal of Materials Chemistry A*, 2013, **1**, 8007.

39. T. Sun, Q. Wu, R. Che, Y. Bu, Y. Jiang, Y. Li, L. Yang, X. Wang and Z. Hu, *ACS Catalysis*, 2015, **5**, 1857-1862.

40. B. Cao, J. C. Neuefeind, R. R. Adzic and P. G. Khalifah, *Inorganic chemistry*, 2015, **54**, 2128-2136.

41. H. Peng, F. Liu, X. Liu, S. Liao, C. You, X. Tian, H. Nan, F. Luo, H. Song, Z. Fu and P. Huang, *ACS Catalysis*, 2014, **4**, 3797-3805.

42. S. Pylypenko, S. Mukherjee, T. S. Olson and P. Atanassov, *Electrochimica Acta*, 2008, **53**, 7875-7883.

43. W. Zhou, X.-J. Wu, X. Cao, X. Huang, C. Tan, J. Tian, H. Liu, J. Wang and H. Zhang, *Energy & Environmental Science*, 2013, **6**, 2921.

44. J. G. Chen, *Chem Rev*, 1997, **96**, 1477-1498.

45. J. K. Norskov, J. Rossmeisl, A. Logadottir, L. Lindqvist, J. R. Kitchin, T. Bligaard and H. Jonsson, *Journal of Physical Chemistry B*, 2004, **108**, 17886-17892.

Graphical Abstract

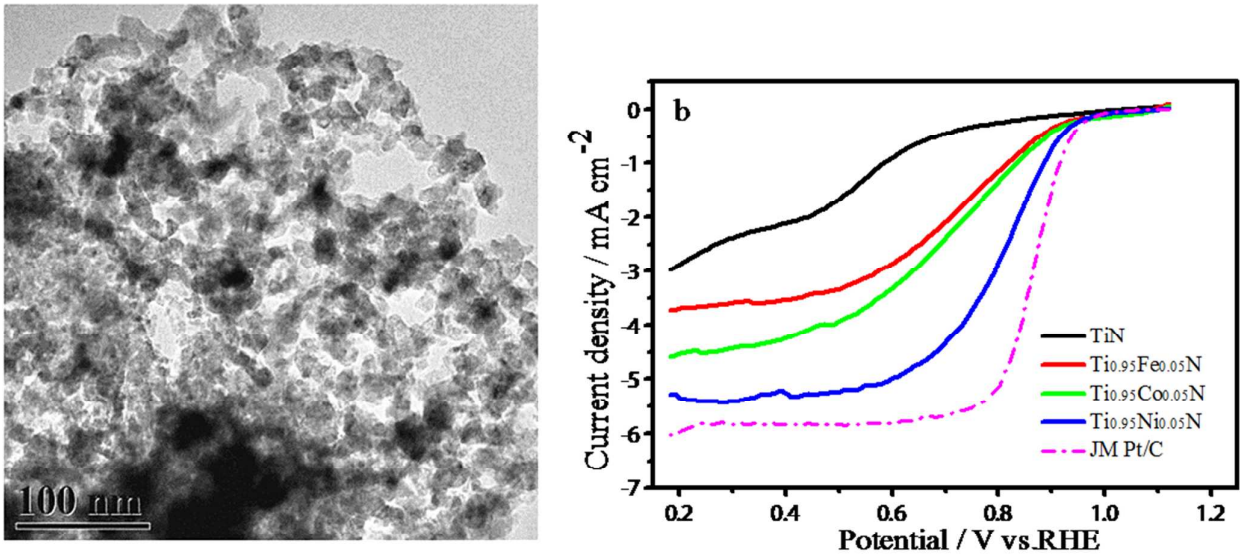

Binary transition metal nitrides demonstrate high activity and stability/durability for the oxygen reduction reaction in both acid and alkaline mediums.